Enhancement cavities for zero-offset-frequency pulse trains

S. Holzberger,[1,2,*] N. Lilienfein,[1,2] M. Trubetskov,[1] H. Carstens,[1,2] F. Lücking,[2] V. Pervak,[2] F. Krausz,[1,2] and I. Pupeza[1,2]

[1]Max-Planck-Institut für Quantenoptik, Hans-Kopfermann-Str. 1, Garching 85748, Germany

[2]Ludwig-Maximilians-Universität München, Am Coulombwall 1, Garching 85748, Germany

*Corresponding author: simon.holzberger@mpq.mpg.de

Received March 24, 2015; accepted April 14, 2015;
posted April 16, 2015 (Doc. ID 236663); published May 4, 2015

The optimal enhancement of broadband optical pulses in a passive resonator requires a seeding pulse train with a specific carrier-envelope-offset frequency. Here, we control the phase of the cavity mirrors to tune the offset frequency for which a given comb is optimally enhanced. This enables the enhancement of a zero-offset-frequency train of sub-30-fs pulses to multi-kW average powers. The combination of pulse duration, power, and zero phase slip constitutes a crucial step toward the generation of attosecond pulses at multi-10-MHz repetition rates. In addition, this control affords the enhancement of pulses generated by difference-frequency mixing, e.g., for mid-infrared spectroscopy. © 2015 Optical Society of America

OCIS codes: (140.4780) Optical resonators; (140.7240) UV, EUV, and X-ray lasers; (300.6340) Spectroscopy, infrared.
http://dx.doi.org/10.1364/OL.40.002165

In a broadband, passive optical resonator, also referred to as enhancement cavity (EC), the ultrashort pulses emitted by a mode-locked laser can be coherently overlapped. If the losses and the phase distortions upon a round-trip inside the EC are low, the steady-state intracavity power can exceed the input power by several orders of magnitude, offering unique advantages for a multitude of applications. Most prominently, ECs have been used to build multi-MHz-repetition-rate sources of coherent extreme-ultra-violet (XUV) radiation by driving high-order harmonic generation (HHG) with kW-average-power-level femtosecond pulses in an intracavity gas target [1–4]. Recently, broadband ECs became relevant to infrared spectroscopy of diluted gases and aerosols. Here, the sensitivity is dramatically improved via resonant enhancement, increasing the effective absorption path length to several kilometers [5–7].

For a given seeding spectrum, a broadband EC dictates the pulse-to-pulse time delay τ and the pulse-to-pulse carrier-to-envelope phase (CEP) slip $\Delta\phi_{\mathrm{cep}}$. An optimum of the enhancement (e.g., for maximizing the intracavity power) is achieved if the seeding pulse train matches both these parameters. In the frequency domain, the pulse train corresponds to a comb of equidistant spectral lines spaced by the pulse repetition frequency $\omega_{\mathrm{rep}}/2\pi = 1/\tau$ and offset from zero by the carrier-envelope offset frequency $\omega_{\mathrm{ceo}} = -(\Delta\phi_{\mathrm{cep}}/2\pi)\omega_{\mathrm{rep}}$ [8,9]. Thus, for a given EC, input spectrum, and optimization criterion, there is an optimal pair of comb parameters, in particular an *optimal offset frequency* (OOF) [5,9,10].

Typically, the parameter ω_{ceo} of the seeding laser is adjusted to fit the OOF dictated by the EC. Some applications, however, require the intracavity pulse to remain unchanged (up to the sign) from round-trip to round-trip, i.e., the phase slip $\Delta\phi_{\mathrm{cep}}$ must be an integer multiple of 2π (or π), corresponding to a comb with zero-offset-frequency (or $\omega_{\mathrm{rep}}/2$). An example is the generation of trains of XUV attosecond pulses or even of isolated attosecond pulses [11], for which zero-slip ECs that simultaneously support short and powerful pulses are a prerequisite. Another example is the enhancement of frequency combs generated via difference-frequency mixing of spectral components originating from the same comb, a process that intrinsically sets ω_{ceo} to zero [6]. Thus, the ability to tune the OOF of a broadband EC is highly desirable and would greatly benefit high-repetition-rate spectroscopic schemes ranging from XUV photoelectron spectroscopy [12] to mid-infrared vibrational spectroscopy [6,7].

In this Letter, we demonstrate the control of the OOF for the enhancement of broadband pulses by employing mirrors with controlled CEP shift upon reflection. This is achieved without sacrificing any other critical parameter, such as high reflectivity, close-to-zero group-delay dispersion (GDD) over a large bandwidth, or high damage threshold. Seeding the EC with nonlinearly broadened and compressed pulses from an Yb-based laser system allows for the enhancement of a zero-offset-frequency pulse train of sub-30-fs pulses to multi-kW-level average powers, limited only by the seed source. Furthermore, our results establish ECs as a simple yet powerful tool to determine the CEP shift imposed on the pulse upon propagation or reflection.

In the steady state and in the absence of any nonlinear medium in the resonator, the electric field of the circulating pulse E_{cav} at the input coupler can be related to the input field E_{in} by the following equation [13]:

$$E_{\mathrm{cav}}(\omega) = \frac{\sqrt{T(\omega)}}{1 - \sqrt{R(\omega)A(\omega)}e^{i\phi(\omega)}} E_{\mathrm{in}}(\omega). \tag{1}$$

Here, we assumed an input coupler of transmission $T(\omega)$ and reflectivity $R(\omega)$. Losses inside the resonator are accounted for by the round-trip power attenuation $A(\omega)$. The spectral phase $\phi(\omega)$ incorporates all phase shifts accumulated upon a round-trip, including those upon reflections from mirrors, transmission through dispersive materials, and geometric phase shifts due to focusing [13]. Maximal power enhancement is reached at

frequencies where the round-trip phase equals a multiple of 2π [see Eq. (1)]. In the presence of GDD, the round-trip phase is not strictly linear in frequency, resulting in varying distances between successive resonances.

In contrast, all spectral lines ω_n of a frequency comb are linear in frequency and given by $\omega_n = n\omega_{\mathrm{rep}} + \omega_{\mathrm{ceo}}$. When coupled to an EC, both comb parameters are adjusted to best fit the equidistant comb to the cavity resonances. For input spectra over which the round-trip phase is sufficiently linear, there is a clear optimum in terms of integrated power enhancement and intracavity pulse duration with respect to ω_{ceo} and ω_{rep}. Although the concept of an OOF is well known [3,5,9,10], control of this parameter has not been reported so far.

In the following, we deduce the round-trip phase slip $\Delta\phi_{\mathrm{cep}}$ experienced by an intracavity pulse given a round-trip phase $\phi(\omega)$ and a laser spectrum $I(\omega)$ [see Fig. 1(a)]. Terms in $\phi(\omega)$ that are proportional to ω merely delay the pulse. Thus, the ϕ-intercept of a linear fit in ω to $\phi(\omega)$ with weights according to the pulse spectrum constitutes the induced phase slip $\Delta\phi_{\mathrm{cep}}$, while the slope represents the group delay τ. Optimal enhancement in this resonator requires a seeding comb with the repetition rate $\omega^*_{\mathrm{rep}} = 2\pi/\tau$ and the offset frequency $\omega^*_{\mathrm{ceo}} = -(\Delta\phi_{\mathrm{cep}}/2\pi)\omega^*_{\mathrm{rep}}$. Hence, we identify the fitted straight line given by $2\pi(\omega - \omega^*_{\mathrm{ceo}})/\omega^*_{\mathrm{rep}}$ with the optimal frequency comb. As the phase is only sampled at the comb lines $\omega_n = n\omega^*_{\mathrm{rep}} + \omega^*_{\mathrm{ceo}}$, the straight line reduces to a series of multiples of 2π. Thus, when evaluating the frequency-resolved power enhancement via Eq. (1), $\phi(\omega_n)$ is equivalent to its deviation from the fit.

One can expand this graphical phase analysis to explain the characteristic shapes of the spectral power enhancement in the case of too high or too low offset frequency of the seeding comb [see Fig. 1(a)]. When sweeping the comb offset frequency while keeping the central region of the input spectrum on resonance—e.g., by deriving the error signal for the locking electronics in that spectral part—the integrated power enhancement traces out a curve with a clear maximum [3,10].

Tuning the phase curve to achieve a desired value of $\Delta\phi_{\mathrm{cep}}$ is possible by manipulating three different contributions to $\phi(\omega)$. First, varying the focusing geometry of the resonator directly changes the Gouy phase $\phi_{n,m} = (m + 1/2)\psi_{\tan} + (n + 1/2)\psi_{\mathrm{sag}}$, which a transverse Gauss–Hermite mode of order n, m acquires per round-trip (in the tangential and sagittal plane, respectively). Here, the Gouy parameters ψ are derived using the $ABCD$-matrix of the resonator according to $\psi = \mathrm{sgn}(B)\arccos[(A + D)/2]$ [13,14]. In spite of the advantage of being continuously adjustable over a large range, in most experiments, the Gouy phase is of limited variability as it is directly linked to the cavity mode size.

Second, inserting a transparent material with a refractive index $n(\omega)$ in the resonator, adds $\omega\tau[n(\omega) - 1]$ to the phase curve. In principle, this can even be done without adding higher-order dispersion, e.g., if a material with an index of refraction according to $n(\omega) = c_1 + c_2/\omega$ with two constants c_1, c_2 is employed. In practice, this is difficult to achieve and is likely to be in conflict with other experimental requirements, such as high vacuum, high damage threshold, polarization insensitivity, or low losses and, thus, limits its usability.

Third, as shown here, the phase upon reflection off the cavity mirrors can be tailored without altering higher order dispersion terms. In this study, we employ coating designs based on quarter-wave stacks, which are widely used as highly reflecting mirrors in ECs. They provide low dispersion at a manageable design complexity and exhibit high damage thresholds. To maximize the bandwidth of the coatings, Nb_2O_5 and SiO_2 are chosen as coating materials due to their large contrast in the refractive indices [15]. The topmost layers of the coating deviate from quarter-wave thicknesses and serve as phase correctors. Besides increasing the spectral width of GDD $<$ 0.5 fs^2 to 96 nm, this opens the possibility to vary the phase slip imprinted on the pulse upon reflection. For the experiment, we implemented two different designs named A and B, differing in $\Delta\phi_{\mathrm{cep}}$. A systematic study of the design optimization for a target value for $\Delta\phi_{\mathrm{cep}}$ exceeds the scope of this Letter.

The experimental setup is sketched in Fig. 1(b). The pulses are generated by the laser system described in [16], delivering 180-fs pulses at a repetition rate of 77 MHz, centered at a wavelength of 1045 nm. Subsequent spectral broadening in a photonic-crystal fiber and compression using chirped mirrors yields close-to-Fourier-limited pulses of 28 fs at a maximum output power of 20 W. The comb offset frequency of the oscillator is freely running with a typical linewidth of ~50 kHz, monitored using an f–$2f$ interferometer. Slow drifts in the offset frequency appearing on the time scale of several minutes are manually compensated by a pair of intra-oscillator wedges. The EC is implemented in a bow-tie configuration equipped with an input coupler with 1% transmission dominating the cavity losses. Due to geometric constraints of the vacuum chamber, a minimum of six cavity mirrors is required in the experiment, although less cavity mirrors would increase the supported bandwidth. If not stated otherwise, the cavity is operated close to the inner edge of the stability range, ensuring nearly identical spot sizes on all mirrors.

We determined the OOF of a cavity configuration by recording the steady-state power enhancement while locking the repetition rate of the input laser to the cavity for different comb offset frequencies. Figure 2(a) demonstrates the tunability of the OOF of a broadband EC by controlling the phase of the highly reflecting cavity mirrors. To this end, we measured the OOF of the EC while

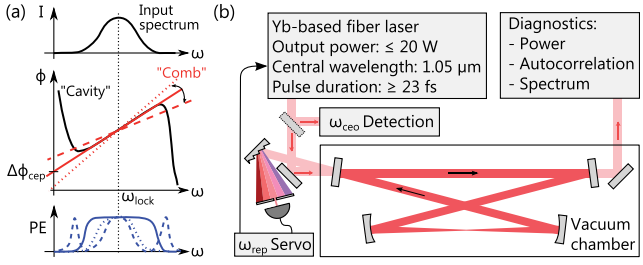

Fig. 1. (a) Upper panel: input power spectrum. Center panel: sketch of the single-round-trip phase $\phi(\omega)$ and of the resulting pulse-to-pulse phase slip $\Delta\phi_{\mathrm{cep}}$. Dashed and dotted lines indicate input comb with too high or too low offset frequency. Lower panel: corresponding spectral power enhancement (PE) in the three cases. (b) Experimental setup.

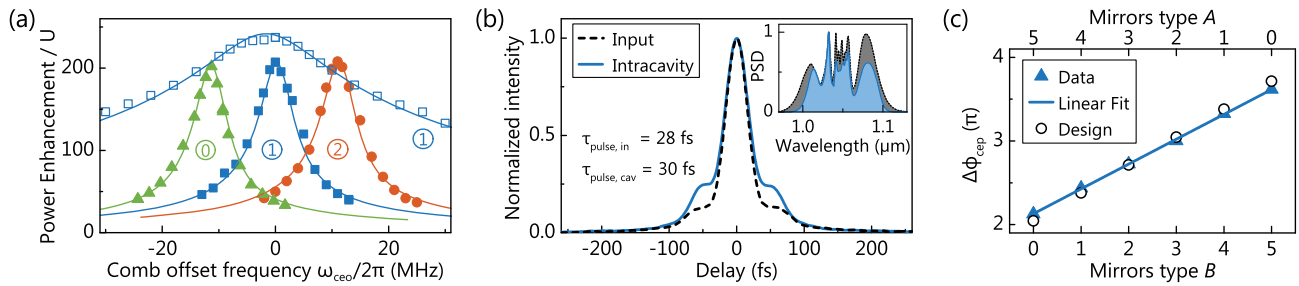

Fig. 2. (a) Power enhancement corrected for the spatial overlap (U) vs. offset frequency of the seeding comb for a cavity employing 0, 1, or 2 mirrors of type *B* (indicated by the numbers). Solid symbols: broadband input pulses. Open symbols: input pulses of reduced bandwidth, illustrating the dependence of the OOF on the spectrum. Solid lines: corresponding model results. (b) Intensity autocorrelation trace of the pulses in case of optimal comb parameters. Inset: corresponding normalized power spectral density (PSD) with 100-nm intracavity bandwidth at −10 dB. (c) Retrieved CEP-shift upon reflection off five cavity mirrors and calculated values from the coating design.

stepwise replacing cavity mirrors of type *A* by mirrors of type *B*. A constant shift of the OOF is observed, in particular reaching zero, when only one mirror of type *B* was employed. For all mirror combinations, a power enhancement of more than 200 was reached with optimal comb parameters. Here, the FWHM of the intensity autocorrelation of the intracavity pulse was measured to be 43 fs, corresponding to a pulse duration of 30 fs assuming a deconvolution factor of 1.41 [see Fig. 2(b)]. Repeating the measurement of the OOF with pulses of a reduced spectral width of ∼8 nm confirms that the sensitivity of the cavity to the comb offset frequency strongly depends on the bandwidth of the pulses. The necessary precision in controlling the round-trip phase and the seeding laser phase noise scales with the bandwidth and with the finesse.

To quantify the CEP slip imprinted upon reflection off a single mirror, we inserted two supplementary mirrors and measured the change in OOF for three combinations of the additional mirrors. The retrieved phase slip of a mirror of type *A* was 1.34 rad, and 2.25 rad in case of type *B*. Both differ by less than 80 mrad from their design values. To proove the reproducibility of our approach, i.e., that all mirrors from one coating run (*A* or *B*) are identical, we plot the measured phase differences and the expected ones in Fig. 2(c). The excellent linear fit to the data, which is also in good agreement with the calculated values, clearly validates the reproducibility.

In Fig. 3(a), the phase slip introduced by Gaussian beam propagation through free space is shown. By

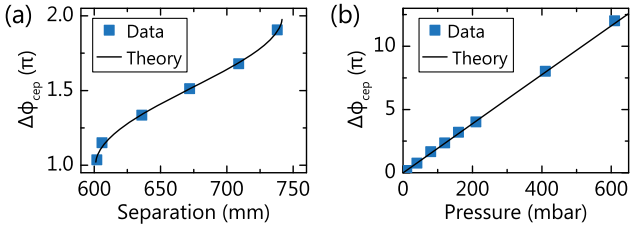

Fig. 3. Dependence of the optimal pulse-to-pulse phase slip $\Delta\phi_{cep}$ on (a) the resonator geometry by varying the separation between the curved mirrors (radius of curvature: −600 mm) and (b) on the argon pressure in the chamber. In (b), input pulses of ∼8 nm bandwidth were used to avoid spectral narrowing. A global offset was added to the data.

stepwise increasing the separation between the curved mirrors, we varied the position of the EC in the stability range and, thus, the Gouy parameter. For each cavity geometry we recorded the OOF. The experimental results excellently agree with theory. If the cavity mode size is not a critical parameter, the Gouy phase constitutes an option to fine-tune the OOF.

In Fig. 3(b), the dependence of the phase slip on the gas dispersion is plotted. By gradually introducing argon gas in the vacuum chamber one can widely tune the OOF. However, the higher order dispersion terms also lead to spectral narrowing of the intracavity spectrum. In the case of broadband, 30-fs pulses and for our finesse, about 0.1 fs^2 of additional GDD is tolerable without sacrificing the intracavity pulse duration. Given the dispersion of argon, this transfers to about 3 mbar of tolerable gas pressure and thus a maximal shift in $\Delta\phi_{cep}$ of about 0.06π. Similarily, the insertion of, e.g., a pair of thin sapphire wedges (<4 μm), is tolerable and would allow for a phase tunability of 0.15π. A robust implementation of such a thin wedge was demonstrated by optically contacting it to a mirror [17].

Using the full input power of the laser, the intracavity power surpassed 3 kW with 30-fs intracavity pulses. Shorter input pulses resulting from stronger nonlinear broadening in the fiber led to slightly shorter intracavity pulses, however at significantly reduced power enhancement. Employing an input coupler with a transmission of 3%, we obtained sub-25-fs pulses at average powers exceeding 1 kW, limited by the power of the seed source. The damage threshold of the mirror coating was determined to be on the order of 1×10^{11} W cm^{-2} using a spot size of 200 μm at pulse durations of 30 fs. The RMS stability of the intracavity power was typically better than 0.25% in the range from 2.5 Hz to 5 MHz, limited by the free-running offset frequency of the laser.

In conclusion, we have designed, produced, and characterized low-loss, broadband mirrors that shift the CEP of a pulse upon reflection in a controlled way. To the best of our knowledge, this is the first demonstration of the control over this degree of freedom of the mirror phase. Using these phase-controlled mirrors, we operated a high-finesse, non-polarization-discriminating EC that supports pulses of 30 fs at a power enhancement of 200, with vanishing pulse-to-pulse phase slip. Through

careful design, neither the bandwidth nor the damage threshold of the mirrors is compromised by the additional "control knob." We showed that nonlinearly broadened and compressed Yb-based master-oscillator-power-amplifier systems are a viable route for reaching multi-kW level pulses of sub-30-fs duration.

With state-of-the art high-power laser systems and thermally robust cavity geometries with even larger mode radii [18], scaling the intracavity power by at least one order of magnitude at similar pulse durations seems straightforward. A further increase of the cavity bandwidth should be feasible by using mirrors with complementary phase characteristics. When equipped with an XUV output coupler as shown in [4], our setup enables the generation of XUV attosecond pulse trains at multi-MHz repetition rates. In addition, for the first time, these pulse parameters and the polarization insensitivity fulfill the prerequisites for the generation of isolated attosecond pulses in ECs via gating mechanisms restricting the XUV emission process to a single event per driving pulse [19,20].

We thank the fiber laser group at the Institute of Applied Physics at Friedrich-Schiller-University Jena for providing the laser system. We acknowledge financial support by the DFG Cluster of Excellence, Munich Centre for Advanced Photonics (MAP) and by the MEGAS Fraunhofer-/Max-Planck-Gesellschaft cooperation. IP acknowledges funding by the European Research Council under grant agreement no. [617173] ACOPS.

References

1. C. Gohle, T. Udem, M. Herrmann, J. Rauschenberger, R. Holzwarth, H. A. Schuessler, F. Krausz, and T. W. Hänsch, Nature **436**, 234 (2005).
2. A. Cingöz, D. C. Yost, T. K. Allison, A. Ruehl, M. E. Fermann, I. Hartl, and J. Ye, Nature **482**, 68 (2012).
3. A. K. Mills, T. J. Hammond, M. H. C. Lam, and D. J. Jones, J. Phys. B **45**, 142001 (2012).
4. I. Pupeza, S. Holzberger, T. Eidam, H. Carstens, D. Esser, J. Weitenberg, P. Rußbüldt, J. Rauschenberger, J. Limpert, T. Udem, A. Tünnermann, T. W. Hänsch, A. Apolonski, F. Krausz, and E. Fill, Nat. Photonics **7**, 608 (2013).
5. F. Adler, M. J. Thorpe, K. C. Cossel, and J. Ye, Annu. Rev. Anal. Chem. **3**, 175 (2010).
6. A. Schliesser, N. Picqué, and T. W. Hänsch, Nat. Photonics **6**, 440 (2012).
7. A. Foltynowicz, P. Masłowski, A. J. Fleisher, B. J. Bjork, and J. Ye, Appl. Phys. B **110**, 163 (2013).
8. S. T. Cundiff, J. Phys. D **35**, R43 (2002).
9. L. Arissian and J. C. Diels, J. Phys. B **42**, 183001 (2009).
10. A. Schliesser, C. Gohle, T. Udem, and T. W. Hänsch, Opt. Express **14**, 5975 (2006).
11. F. Krausz and M. Ivanov, Rev. Mod. Phys. **81**, 163 (2009).
12. A. Stolow, A. E. Bragg, and D. M. Neumark, Chem. Rev. **104**, 1719 (2004).
13. A. E. Siegman, *Lasers* (University Science Books, 1986).
14. J. Weitenberg, P. Rußbüldt, I. Pupeza, T. Udem, H.-D. Hoffmann, and R. Poprawe, J. Opt. **17**, 025609 (2015).
15. S. A. Furman and A. V. Tichonravov, *Basics of Optics of Multilayer Systems* (Editions Frontières, 1992).
16. T. Eidam, F. Röser, O. Schmidt, J. Limpert, and A. Tünnermann, Appl. Phys. B **92**, 9 (2008).
17. I. Pupeza, E. E. Fill, and F. Krausz, Opt. Express **19**, 12108 (2011).
18. H. Carstens, N. Lilienfein, S. Holzberger, C. Jocher, T. Eidam, J. Limpert, A. Tünnermann, J. Weitenberg, D. C. Yost, A. Alghamdi, Z. Alahmed, A. Azzeer, A. Apolonski, E. Fill, F. Krausz, and I. Pupeza, Opt. Lett. **39**, 2595 (2014).
19. P. Tzallas, E. Skantzakis, C. Kalpouzos, E. P. Benis, G. D. Tsakiris, and D. Charalambidis, Nat. Phys. **3**, 846 (2007).
20. X. Feng, S. Gilbertson, H. Mashiko, H. Wang, S. D. Khan, M. Chini, Y. Wu, K. Zhao, and Z. Chang, Phys. Rev. Lett. **103**, 183901 (2009).